RESEARCH PAPER

PCCP
www.rsc.org/pccp

Mechanism and rate of the reaction $CH_3 + O$—revisited

W. Hack,[a] M. Hold,[b] K. Hoyermann,[b] J. Wehmeyer[b] and T. Zeuch*[b]

[a] *Max-Planck-Institut für Biophysikalische Chemie, Göttingen, Germany*
[b] *Institut für Physikalische Chemie, Georg-August-Universität, Göttingen, Germany. E-mail: jkupfer@gwdg.de*

Received 21st December 2004, Accepted 15th March 2005
First published as an Advance Article on the web 7th April 2005

The primary products and the rate of the reaction of methyl radicals with oxygen atoms in the gas phase at room temperature have been studied using three different experimental arrangements: (A) laser flash photolysis to produce CH_3 and O from the precursors CH_3I and SO_2 (the educts and the products were detected by quantitative FTIR spectroscopy); (B) the coupling of a conventional discharge flow reactor *via* a molecular sampling system to a mass spectrometer with electron impact ionization, which allowed the determination of labile and stable species; (C) laser induced multiphoton ionization combined with a TOF mass spectrometer–molecular beam sampling–flow reactor, which was used for the specific and sensitive detection of the CH_3, CD_3, C_2H_5 and C_2D_5 radicals and the determination of rate coefficients. The branching ratio of the reaction channels was determined by the experimental arrangements (A) and (B) leading to $CH_3 + O \rightarrow HCHO + H$ (55 ± 5)% $\rightarrow CO + H_2 + H$ (45 ± 5)%. The rate coefficients of the normal and deuterated methyl and ethyl radicals with atomic oxygen showed no isotope effect: $k(CD_3 + O)/k(CH_3 + O) = 0.99 \pm 0.12$, $k(C_2D_5 + O)/k(C_2H_5 + O) = 1.01 \pm 0.07$ (statistical error, 95% confidence level). The absolute rate coefficient of the reaction $CH_3 + O$ was derived with reference to the reaction $C_2H_5 + O$ ($k = 1.04 \times 10^{14}$ cm^3 mol^{-1} s^{-1}) leading to $k(CH_3 + O) = (7.6 \pm 1.4) \times 10^{13}$ cm^3 mol^{-1} s^{-1}.

Introduction

Methyl radicals are essential radicals in the oxidation of hydrocarbons, which is obvious by considering different scenarios. Natural gas for heating purposes consists mainly of methane, which is primarily attacked in an oxidation process by atoms (H, O) and radicals (OH) to yield methyl radicals. At high temperatures the global mechanism of the oxidation of higher alkanes includes, as the main route, the thermal decomposition of the higher alkyl radicals to give methyl and ethyl radicals (see for example ref. 1). In a combustion process the concentration of oxygen atoms is often well below that of molecular oxygen but the rate coefficients of $k(O + CH_3, C_2H_5)$ may exceed those of $k(O_2 + CH_3, C_2H_5)$ by several orders of magnitude. Therefore in flames, for example, the fate of the methyl radical is strongly governed by the attack of the oxygen atoms. Two aspects of the title reaction $CH_3 + O$ are of vital importance for the understanding and modeling of the combustion of hydrocarbons: the primary products and the rate coefficient of this reaction. Numerous theoretical and experimental studies report on the mechanism

$$CH_3 + O \rightarrow CH_3O^* \quad (1)$$

$$CH_3O^* \rightarrow HCHO + H \quad (a_1)$$

$$\rightarrow CO + H_2 + H \quad (a_2)$$

and on the rate coefficient.

A short but incomplete summary is listed in Table 1. Previous studies state an overwhelming contribution of (a_1) to the total reaction (>95%, refs. 2–5), recent studies, however, have reported lower contributions for (a_1) and higher for (a_2), (refs. 6, 7, 9–11, 13 and 15). The reported rate coefficients as measured or evaluated otherwise show values between *ca.* (7–11) × 10^{13} cm^3 mol^{-1} s^{-1}. A more recent theoretical study states agreement with the experimental studies of Fockenberg and Preses[10] in respect to the rate coefficient.[14] Data compilations[15,16] recommend $k = 8.4 \times 10^{13}$ cm^3 mol^{-1} s^{-1}.

The importance of reaction (1) for a quantitative description of the oxidation of alkanes, where the methane oxidation is the main building block in the hierarchy, motivates additional measurements of this fundamental reaction. Since all the experimental techniques which have been used in previous studies have their own virtues and deficiencies, an additional study with the experimental arrangements discussed in the experimental section can be considered as a useful and critical test of the data reported so far.

The objectives of the present study are to elucidate the reaction mechanism by measuring the primary products of both channels (a_1) and (a_2) using different experimental arrangements and to determine the rate coefficient of the overall reaction (1).

Experimental

Three independent experimental arrangements and procedures have been applied. In order to keep the paper short only a brief description is given here.

Arrangement (A)

A laser flash photolysis cell (pressure: 3 mbar to 1 bar) with an internal multiple path mirror arrangement is directly coupled to a FTIR spectrometer for a quantitative concentration determination of the reactants. The labile species CH_3 and O are produced from the precursors CH_3I and SO_2 by co-photolysis at 193 nm.[17,18] As the determination of the formed HCHO is crucial for the evaluation of the branching ratio and as the absolute calibration of HCHO is susceptible to errors caused by losses at the wall and by polymerization, an extensive calibration program was performed. The consumed amount of the precursor CH_3I was determined and all C atom-bearing products were identified and calibrated. The recovery of the

DOI: 10.1039/b419137d

Table 1 The reaction $CH_3 + O$: previous results

Channel fraction HCHO (%)	Channel fraction CO (%)	k/cm^3 mol^{-1} s^{-1} at 289 K	Ref.
>95	—	—	2
100	—	8.43×10^{13} (±20%)	3
100	—	—	4
100	—	—	5
—	40 ± 10	—	6
—	17 ± 11	1.07×10^{14} (±17%)	7
—	18 ± 4	—	9
84 ± 12	15 ± 6	7.34×10^{13} (±13%)	10
55 ± 6	45 ± 6	8.00×10^{13} (±15%)	11
—	—	7.83×10^{13} (±15%)	12
—	—	1.02×10^{14} (±20%)	13
—	—	9.26×10^{13} (±10%)	14
100	—	8.43×10^{13} (*ca.* ±50%)	15
60	40	8.4×10^{13}	3,6,16

total carbon mass was 95–98%. Moreover, the absorption cross sections of SO_2 and CH_3I at the laser emission line (193.2 nm, half-width 1.3 nm) were carefully measured in our reaction cell (known path length, laser-beam energy monitored for different substance concentrations, SO_2: 252 mol m^{-2}, CH_3I: 48 mol m^{-2}, see also ref. 18) in order to determine the absolute O atom and CH_3 radical start concentrations in the photolytic experiments. By using this arrangement a well defined reaction system could be prepared and final product concentrations could be modeled with a simple kinetic scheme.

Arrangement (B)

A combination of two independently operated conventional discharge flow reactors is connected to the ion source of a magnetic deflection mass spectrometer with electron impact ionization by a molecular beam sampling. The specific detection of labile and stable species was performed by the mass spectrometry at low-energy electron impact ionization (4.5–29.5 eV); by adopting such a value an optimal signal-to-noise ratio was achieved at low mass spectroscopic interference (*i.e.* fragment ion formation). A sensitive detection is achieved by a synchronous single ion counting technique, where the atom/radical producing microwave discharge is switched "on/off", thus preparing the condition of reaction "on/off". CH_3 radicals are formed *via* the reaction of F atoms with CH_4. F and O atoms are produced directly by discharging highly diluted F_2/He and O_2/He mixtures.[19]

Arrangement (C)

Rate coefficients were determined by a combination of discharge flow reactors and a TOF-mass spectrometer where the radicals are detected specifically and sensitively *via* the laser induced multiphoton ionization.[20] Chemicals were of commercial grade: (He(≥ 99.995%), Ar (≥ 99.6%, SO_2 (≥ 99.98%), CO(≥ 98%), CH_4 (≥ 99.995%), O_2 (≥ 99.995%), He/F_2 (99.995%/98%), all Messer-Griesheim; $CFCl_3$ (≥ 99.5%), CH_3I (≥ 99%), Fluka; CD_4 (≥ 98 atom% D), C_2D_6 (≥ 99 atom% D), Aldrich).

Results and discussion

Primary products

The determination of the primary products by arrangement (A) is based on the IR spectra in the region 600–5000 cm^{-1} after the co-photolysis of CH_3I/SO_2 mixtures. In order to unravel the spectra, characteristic regions with minimal spectral interferences were chosen for identifying and quantifying the contributions of the precursors and their consumption (CH_3I, SO_2), of the primary products, and of the by-products (C_2H_6, CH_4, C_2H_4, S_2O, $(SO)_2$).

Table 2 The reaction mechanism of $CH_3 + O$, data compiled from refs. 15 and 25

Reaction			k/cm^3 mol^{-1} s^{-1}
$CH_3 + O$	→	$HCHO + H$	4.2×10^{13}
$CH_3 + O$	→	$CO + H_2 + H$	3.4×10^{13}
$CH_3 + CH_3$	→	C_2H_6	2.8×10^{13}
$CH_3 + H$	→	CH_4	5.0×10^{13}
$CH_3 + OH$	→	CH_3OH	5.0×10^{13}
$CH_3 + I$	→	CH_3I	7.0×10^{12}
$CH_3I + O$	→	$CH_3 + IO$	4.7×10^{12}
$CH_3I + H$	→	$CH_3 + HI$	4.0×10^{12}
$CH_3I + OH$	→	$CH_2I + H_2O$	4.4×10^{10}
$HCHO + O$	→	$OH + CO + H$	1.0×10^{11}
$HCHO + OH$	→	$H_2O + CO + H$	5.5×10^{12}
$HCHO + H$	→	$CO + H_2 + H$	3.0×10^{10}
$CH_3O + O$	→	$CH_3 + O_2$	1.5×10^{13}
$CH_3O + O$	→	$HCHO + OH$	6.0×10^{12}
$CH_3O + H$	→	$HCHO + H_2$	1.8×10^{13}
$IO + O$	→	$O_2 + I$	7.2×10^{13}
$IO + IO$	→	$O_2 + I_2$	3.0×10^{12}
$IO + IO$	→	$O_2 + I + I$	3.2×10^{12}
$OH + O$	→	$O_2 + H$	2.0×10^{13}
$OH + OH$	→	$H_2O + O$	1.1×10^{12}
$OH + H$	→	H_2O	1.0×10^{10}
$OH + C_2H_6$	→	$C_2H_5 + H_2O$	1.5×10^{11}
$CH_2I + CH_2I$	→	$C_2H_4I_2$	2.4×10^{13}

The hydrocarbons C_2H_6, CH_4, C_2H_4 and their formation as by-products are explained by the reactions listed in Table 2. Their contributions were quantified at the characteristic wavelength regions (CH_4 around 3000 cm^{-1}, rotational resolved; C_2H_6: 2950–3000 cm^{-1}, rotational resolved, C_2H_4: 954 cm^{-1}.) A peak at 1160 cm^{-1} is assigned to S_2O as peaks at 1169/679 cm^{-1} are known from calculations[21] and the peak at 2060 is also assigned to a sulfur-bearing by-product such as $(SO)_2$ or an overtone of S_2O.

Fig. 1 shows an example of the extracted product spectra of CO (Fig. 1c) and HCHO (Fig. 1b) obtained by subtracting the contributions of the calibrated by-product concentrations from the reduced product spectrum (Fig. 1a). As illustrated in Fig. 1d the net absorption in the fingerprint region of C–C compounds (around 850–1150 cm^{-1}) levels off indicating that these compounds were correctly taken into account. The deduced CO spectrum from the overall spectrum matches the pure CO spectrum. The CO yield was determined by recording spectra for each pressure relevant to the experimental conditions and the product spectra were compared to this spectra–concentration set. By this, saturation effects due to the limited spectral resolution of the rotational CO-bands are avoided. The extracted HCHO spectrum from the measurements (Fig. 1b) coincides perfectly with the features of spectral position and line strength of a HCHO spectrum reported in the literature[22] (2843 cm^{-1}, 2783 cm^{-1}, 1746 cm^{-1}, 1500 cm^{-1}). This is taken as evidence that all carbon containing species were correctly assigned and quantified. Therefore the absolute HCHO concentration was derived from the total carbon mass balance, leading to an experimental calibration factor of the HCHO concentration. It is noteworthy to state that this calibration factor has been applied also to the determination of the HCHO yield of the reaction $C_2H_5 + O$ (2): $C_2H_5 + O \rightarrow C_2H_5O^*$

$$C_2H_5O^* \rightarrow HCHO + CH_3 \quad (2a_1)$$

$$\rightarrow CH_3CHO + H \quad (2a_2)$$

$$C_2H_5 + O \rightarrow C_2H_4 + OH \quad (2b)$$

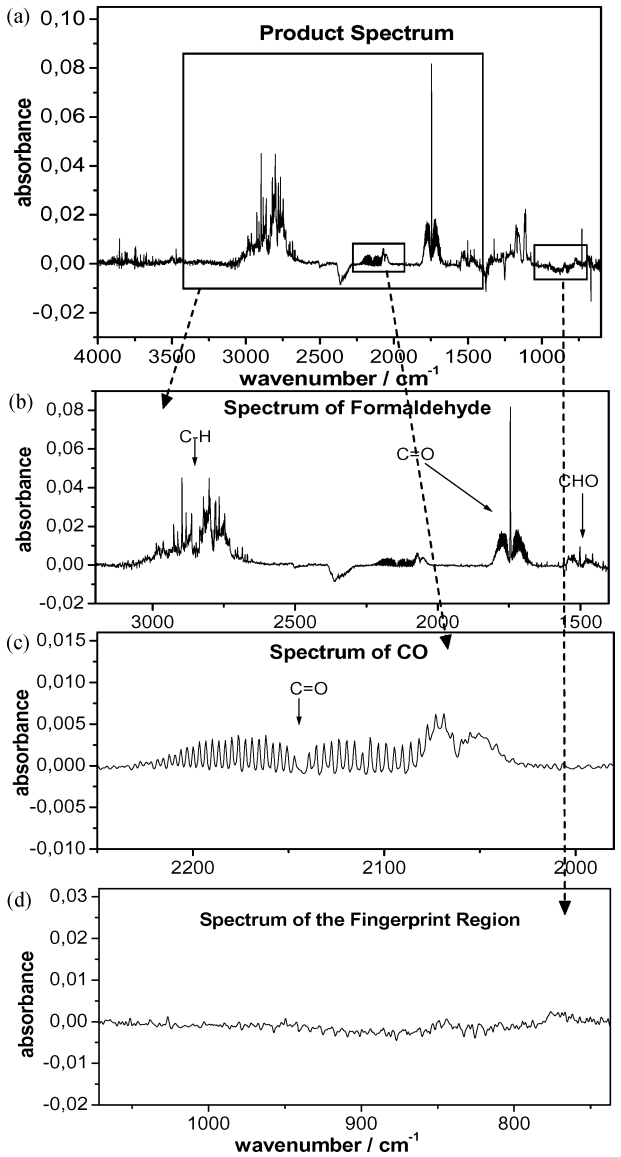

Fig. 1 The reaction $CH_3 + O$: (a) formation of the products HCHO and CO as measured by FTIR spectroscopy; (b) and (c) extracted spectra of HCHO and CO, respectively; (d) fingerprint region of C–C species ($p = 4.0$ mbar, $T = 293$ K, $p(CH_3I) = 0.4$ mbar, $p(SO_2) = 1.4$ mbar, $p(Ar) = 2.2$ mbar, 200 laser shots, energy around 80 mJ per shot when coupled to the cell, averaged over 200 scans).

The branching ratio of the reaction channels HCHO + CH_3 (xa$_1$)/CH_3CHO + H (xa$_2$) has been reported in the literature to be: (xa$_1$)/(xa$_2$) = 0.80 (experimental),[23] 0.91 (theoretical).[19] Our experimental value,[18] based on the calibration factor derived here, is (x(a$_1$))/(x(a$_2$)) = 0.73. This agreement in the HCHO formation for the reaction $C_2H_5 + O$ gives indirect support for the determination of the HCHO yield for the reaction $CH_3 + O$. In Figs. 2a, 2b and 2c the formation of the products HCHO and CO is displayed as a function of the consumption of the precursor CH_3I for different excess ratios of the initial CH_3I and SO_2 concentrations. No systematic dependence of the product yield of HCHO and CO on the applied initial concentration ratio $[CH_3]_0/[O]_0$ is observed, thus an averaging of the product yields seems to be adequate leading to (a$_1$)/(a$_2$) = 55.8/44.2.

The experiments were performed with small and large excess of O over CH_3. As additional CH_3 is quickly formed *via* $CH_3I + O \rightarrow CH_3 + IO$, ref. 24, the actual conditions after 5 μs resulted in a CH_3 excess for $[CH_3I]_0/[SO_2]_0 = 0.6/0.2$ and an O atom excess for $[CH_3I]_0/[SO_2]_0 = 0.4/1.4$. Since the determination of the branching ratio is based on the final

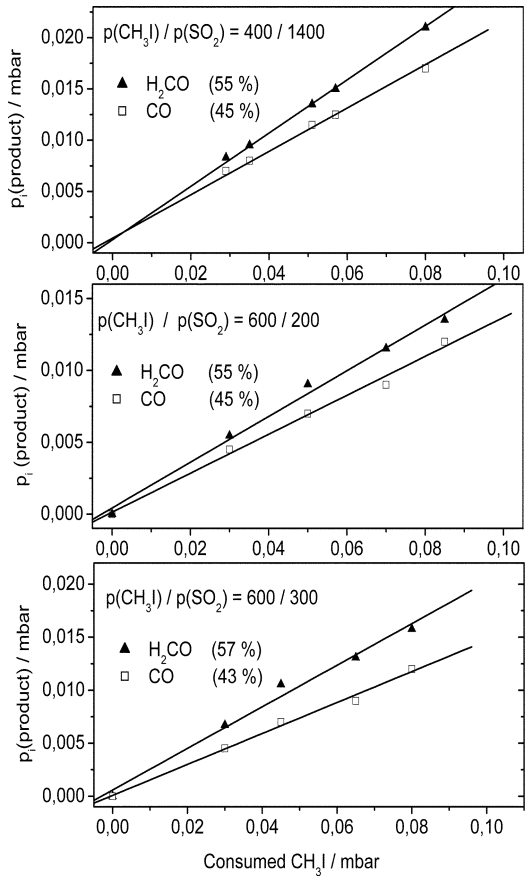

Fig. 2 The reaction $CH_3 + O$: formation of the products HCHO and CO with increasing conversion of the precursors ($p = 4.0$ mbar, $T = 293$ K, initial mixture strength of $[CH_3I]_0/[SO_2]_0 = 0.40/1.40$; 0.60/0.20; 0.60/0.30 mbar, $[CH_3]_0/[O]_0$ ratios were 0.05, 0.57, 0.38).

product analysis, the influence of consecutive and parallel reactions on the branching ratio (a$_1$)/(a$_2$) was studied by modeling the total reaction system along the scheme of Table 2. In Fig. 3 concentration/time profiles are given. Such simulations with the initial experimental conditions (see Fig. 2) show that the primary branching ratio (a$_1$)/(a$_2$) at short reaction times deviates even for the large initial excess of O atoms from the measured one ("final product analysis") by less than 2%, which is well within the experimental error. Therefore reactions such as the O atom or H atom attack on HCHO, which could potentially influence the ratio (a$_1$)/(a$_2$), show no significant impact under the chosen conditions and reactions of IO with molecules are too slow to do so.[26] It is noteworthy that also the final concentrations of CH_4 and C_2H_6 are correctly predicted

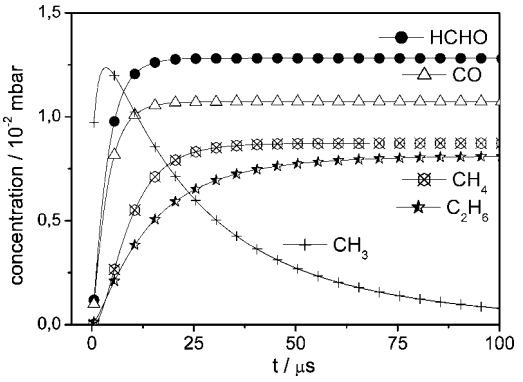

Fig. 3 The reaction $CH_3 + O$: modeling of the concentration/time profiles of species assuming the reactions of Table 2 and the experimental conditions of Fig. 2 ($[CH_3I]_0/[SO_2]_0 = 0.40$ mbar/1.4 mbar, $[CH_3]_0 = 0.9 \times 10^{-2}$ mbar, $[O]_0 = 0.18$ mbar).

by the model for low and high initial O atom excess. Together with the scatter of the measurements (statistical regression errors, 95% confidence interval, each graph was taken and averaged over the three experiments) this leads to error margins of $(a_1)/(a_2) = (55.8 \pm 5.6)/(44.2 \pm 5.6)$.

By independent measurements *via* the experimental set up (B), the formation of CO together with the consumption of CH_3 radicals by O atoms was followed by time-resolved mass spectrometry, applying low absolute radical concentrations ($<10^{-10}$ mol cm^{-3}) and small detection times (<2 ms). The quantitative determination of the formation of CO was performed at an ionization energy of 24 eV at $m/z = 28$, leading to a good compromise with respect to sensitivity, specifity and fragmentation (*e.g.* $HCHO^+ \rightarrow HCO^+$, CO^+). Absolute CH_3 concentrations were derived from the controlled mass flow of CH_4 and the consumption by the F atoms. At the mass peak of CO ($m/z = 28$) only a minor contribution of HCHO (<6%) was observed. A contribution of C_2H_6 was absent as C_2H_6 formation according to $CH_3 + CH_3 \rightarrow C_2H_6$ was suppressed by the low absolute CH_3 concentrations. A small background signal at $m/z = 28$ was attributed to air leaks (N_2) and to CO produced *via* $CH_3 + O$ with O atoms from the discharge of the (F_2/He) mixture with an air impurity. The extensive mass spectroscopic calibration procedures for the stable species are based on Ar as an internal reference standard. In order to illustrate the data reduction and the extent of corrections an example is given in Fig. 4. The evaluation of the production of CO per reacted CH_3 radical with O atoms gave $(+\Delta[CO])/(-\Delta[CH_3]) = (46 \pm 6)\%$. Thus the branching ratio of $(a_2)/(\sum(a_i)) = (46 \pm 6)\%$ is in good agreement with the results obtained by the flash photolysis–FTIR study.

Our presented determination of the branching ratio $(a_2)/(a_1)$ as obtained by the two independent experimental arrangements differing in the reactor (static photolysis cell/flow reactor) and the analytical tool (FTIR spectroscopy/mass spectrometry), matches the results of Seakins and Leone.[6] Their value of 40% for channel (a_2) was derived from time-resolved FTIR emission spectrocopy of CO*. This technique probes the nascent formation of products such as CO* or OH* as convincingly demonstrated and discussed by Leone *et al.* in several papers.[6,9,27,28] However, lower values for the contribution of the CO formed *via* route (a_2) were obtained from experiments with other techniques ((17 ± 11)%, flow reactor-photoionization mass spectrometer (TOFMS-PI),[7] (18 ± 4)%, photolysis cell-diode laser absorption,[8] (15 ± 6)%, flow reactor-TOFMS-PI[10]). A theoretical study[9] favours these lower values for the efficiency of CO formation.

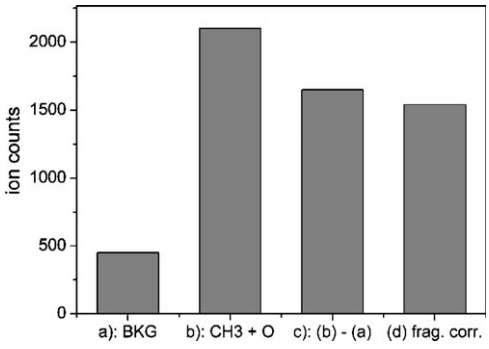

Fig. 4 The reaction $CH_3 + O$: formation of CO as studied by the mass spectrometric arrangement (B). Ion signals at $m/z = 28$ for the following conditions in the flow reactor: (a) presence of CH_3 radicals (discharge "on" for F_2/He → F/He, reaction $F + CH_4 \rightarrow CH_3 + HF$; discharge "off" for O_2/He), "background" BKG; (b) presence of CH_3 radicals and O atoms (discharge "on" for F_2/He → F/He, reaction $F + CH_4 \rightarrow CH_3 + HF$; discharge "on" for O_2/He → O/He; (c) difference of the ion signals of (b) − (a), "corrected for background signal"; (d) correction of signal (c) due to fragment ion formation of HCHO at $m/z = 28$, "net CO formation".

As already emphasized in the introduction our presented experimental study is intended to add new experimental data on the important reaction $CH_3 + O$ and we hesitate to speculate on the virtues and deficiencies of the experimental techniques applied so far. Moreover, we do not feel qualified to analyze the theoretical investigations published until now.[5,9] But we point to the high density of states of the chemical highly activated CH_3O^* making a precise theoretical quantification of channel fractions a challenging problem (see refs. 9 and 14).

Rate of reaction

The rate coefficient of the reaction of methyl radicals with oxygen atoms was measured with reference to the reaction of ethyl radicals with oxygen atoms, as the latter is reported as a high quality rate coefficient.[18]

The competitive method for the determination of the ratio of the rate coefficients of the general type

$$R_1 + O \rightarrow \text{products} \quad \text{(i)}$$

$$R_2 + O \rightarrow \text{products} \quad \text{(i0)}$$

can be accomplished by the simple relation

$$k_i/k_{i0} = \ln\{[R_1]_0/[R_1]\}/\ln\{[R_2]_0/[R_2]\} \quad (1)$$

where $[R]_0$ and [R] are the concentrations of the radical R in the absence and in the presence of oxygen atoms, respectively. The precautions to be taken are the absence of other radical removing reactions (radical combination and cross combination) and other radical forming reactions (products of the radical and atomic oxygen reaction). Radical combination reactions can be greatly suppressed when using very low absolute radical concentrations as in the sensitive and specific

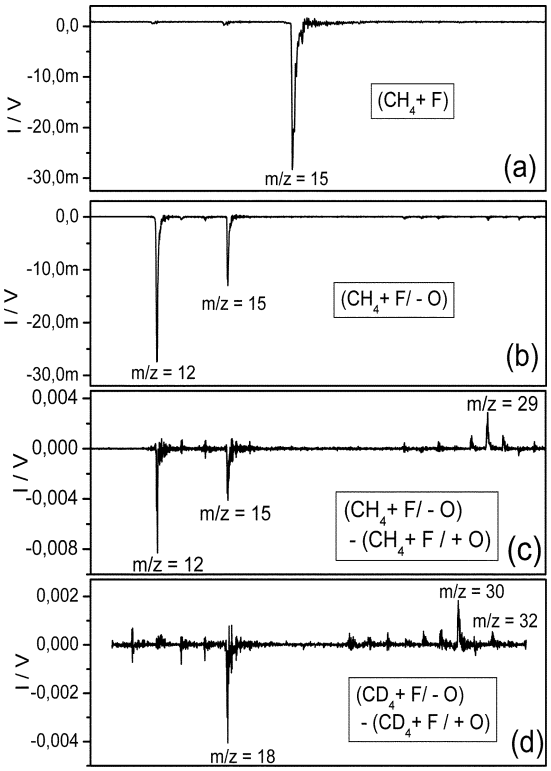

Fig. 5 The reactions $CH_3/CD_3 + O$: detection of the radicals and of the products by mass spectrometry after laser induced multiphoton ionization. (a) CH_3 radical at $\lambda = 450.6$ nm (laser energy: 18 mJ; $p = 1.35$ mbar; $T = 298$ K, $x(CH_4) = 3.8$ mol%, $x(F_2) = 0.15$ mol%; (b) CH_3 radical at $\lambda = 340.8$ (laser energy: 8.5 mJ, $p = 1.73$ mbar, $x(CH_4) = 0.52$ mol%, $x(F_2) = 0.14$ mol%, $x(O_2) = 0.04$ mol%); (c) difference of the mass spectra for the condition "$CH_3 + O$" and "CH_3, absence of O atoms, spectrum (b)"; (d) as (c), CH_3 replaced by CD_3 ($x(CD_4) = 0.52$ mol%).

detection of the CH_3 and C_2H_5 radicals *via* laser induced multiphoton ionization. The interference between CH_3 radical consumption and formation can be avoided by the isotopic substitution of C_2H_5 by C_2D_5 as explained below.

Additionally, the rate coefficients of the atomic oxygen reactions of the fully deuterated CD_3 and C_2D_5 are to be determined. As shown in Figs. 5a and 5b, CH_3 radicals are detected by mass spectrometry and laser induced multiphoton ionization at the wavelength $\lambda = 450.8$ nm ($3d^2E''$, 3 + 1 Rempi band) and $\lambda = 340.8$ nm ($3p^2A_2''$, 2 + 1 Rempi band[29]), showing some ion fragmentation at the lower wavelength. Fig. 5c gives the signal difference of the mass spectra for the conditions of the presence of the CH_3 radicals with and without O atoms, *i.e.* a negative value indicates consumption, a positive one formation due to reaction. The consumption of CH_3 radicals ($m/z = 15$) is accompanied by a signal increase at $m/z = 29$. This is assigned to a fragment ion HCO^+ ($m/z = 29$) produced by the ionization of $HCHO^+ \rightarrow HCO^+ + H$. The equivalent measurements of the deuterated methyl radical CD_3 are displayed in Fig. 5d with a signal decrease at $m/z = 18$ (CD_3) and an increase at $m/z = 30$ (DCO^+, from $DCDO^+ \rightarrow CDO^+ + D$). It is to be noticed that for the conditions of the reaction $CH_3 + O$, no signal is observed at $m/z = 18$ (Fig. 5c) and for $CD_3 + O$ no signal is observed at $m/z = 15$ (Fig. 5d). Therefore no mass spectrometric interference is present for the determination of the ratio of the rate coefficients of the reactions (1) and $CD_3 + O$ (1D), k_1/k_{1D}.

In Fig. 6 the measurements are displayed according to eqn. (1), showing the expected line through the origin with a slope of $k_1/k_{1D} = 1.01 \pm 0.12$, (error limits: statistical error, 95% confidence level).

This means that the reactions (1) and (1D) are equally fast and no isotope effect is observed. A similar result ($k_1/k_{1D} = 1.07 \pm 0.05$) is reported by Washida and Inomata.[13]

Equivalent studies were performed for the reference reactions $C_2H_5 + O$ (2), and $C_2D_5 + O$ (2D). Fig. 7a shows the nearly fragmentionless ionization of C_2H_5 radicals at $\lambda > 400$ nm (here shown at $\lambda = 406$ nm). Care has to be taken in the spectral region of the ionization of NO being produced in small amount due to air leaks in the experimental set up if the microwave discharge is on (signal of NO at $m/z = 30$ at 380–383, 429–431, 452–454 nm). At a lower wavelength ($\lambda = 340.8$ nm), the wavelength for the specific detection of CH_3 and CD_3 radicals, a rich fragmentation pattern is observed (Fig. 7b) ($m/z = 29$, 27, 26, 25, 24, 15, 14). The signal differences of the mass spectra for the reaction $C_2H_5 + O$ and $C_2D_5 + O$ (Fig. 7c and 7d) allow the identification of some primary products of these reactions and the experimental choice for the determination of the rate coefficients. The consumption of C_2D_5 ($m/z = 34$) is accompanied by the formation of CD_3 ($m/z = 18$), DCDO ($m/z = 30$, DCO^+ from DCDO, see also $CH_3 + O$, $CD_3 + O$, Fig. 5) and CD_3CDO ($m/z = 46$, CD_3CO^+ from CD_3CDO, Fig. 7d. These findings reflect the mechanism:[18]

$$C_2D_5 + O \rightarrow C_2D_5O^* \; C_2D_5O^* \rightarrow DCDO + CD_3$$
$$\rightarrow CD_3CDO + D \; C_2D_5 + O \rightarrow C_2D_4 + OD$$

It is noted that no background signal is present at $m/z = 15$ (the mass peak of CH_3) and that the mass peak at $m/z = 34$ (the mass peak of C_2D_5) is not masked by other species or fragment ions. In the study of the reaction $C_2H_5 + O$ (Fig. 7c) the consumption of C_2H_5 ($m/z = 29$) is obscured by HCO^+ from HCHO ($m/z = 29$), but the formation of CH_3 radicals ($m/z = 15$) is clearly detected. In order to determine the ratio of the rate coefficients $k(C_2D_5 + O)/(k(C_2H_5 + O)$ a wavelength of $\lambda = 435$ nm was chosen. Here the mass peaks $m/z = 34$ (C_2D_5) and $m/z = 29$ (C_2H_5) do not interfere with products or fragment ions (HCO^+ from HCHO) and no background of NO is present. Measurements being displayed in Fig. 8 resulted in $k(C_2D_5 + O)/(k(C_2H_5 + O) = 1.01 \pm 0.07$ (linear regression, 95% confidence level). This means that no isotope effect is observed within the experimental error.

The rate of the reaction $CH_3 + O$ was measured with reference to $C_2D_5 + O$. As demonstrated by Figs. 5 and 7 the mass peaks $m/z = 15$ and $m/z = 34$ at $\lambda = 340.8$ nm can be unequivocally assigned to the radicals CH_3 and C_2D_5 thus allowing here the measurement of the consumption of these radicals. The measurements with different absolute radical concentrations, achieved using a low and very low F atom concentration (1.46×10^{-10} and 2.55×10^{-11} mol cm^{-3}, respectively) gave the values (see Fig. 9) $k(CH_3 + O)/k(C_2D_5 + O) = 0.707 \pm 0.08$ ("very low") and 0.592 ± 0.02 ("low").

At very low radical concentrations the condition of suppressing secondary and competitive reactions is approximated at the expense of a larger scatter of the measurements. This

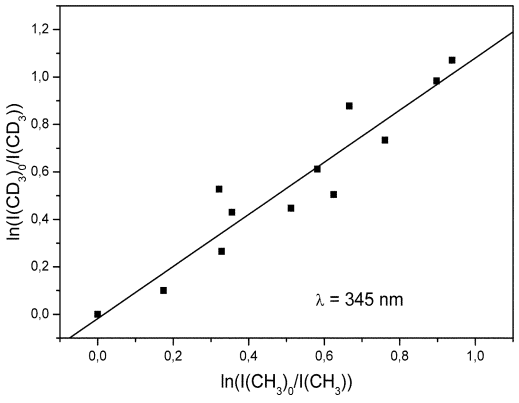

Fig. 6 The reactions $CH_3/CD_3 + O$: determination of the relative rate coefficients of the reactions $CD_3 + O$ and $CH_3 + O$ by the consumption of the radicals for increasing amounts of O atoms. $I_0(R)$, I(R): ion signal of the radical in the absence and in the presence of O atoms, respectively. Arrangement (C): $\lambda = 340.5$ nm; laser energy = 5.5 mJ; $p = 1.76$ mbar; $T = 298$ K, $x(CH_4) = x(CD_4) = 0.96$ mol%, $x(F_2) = 0.14$ mol%, $x(O_2) = 0$–0.27 mol%.

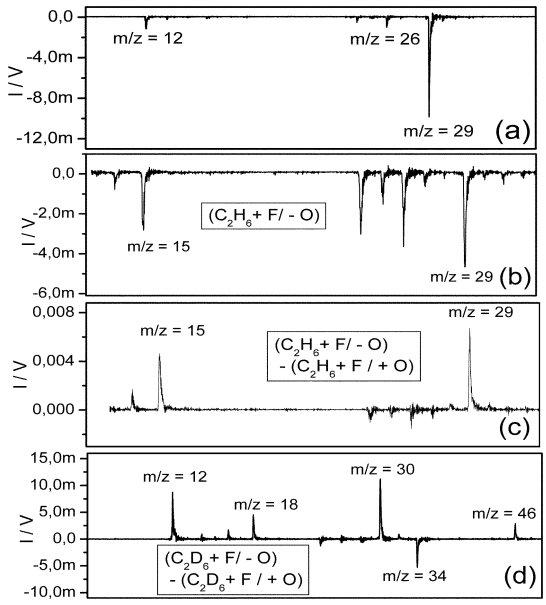

Fig. 7 The reactions $C_2H_5 + O$ and $C_2D_5 + O$: detection of the radicals and the products by mass spectrometry after laser induced multiphoton ionization. (a) C_2H_5 radical at $\lambda = 406.0$ nm (laser energy = 8.5 mJ; $p = 1.78$ mbar, $T = 298$ K, $x(C_2H_6) = 0.88$ mol%, $x(F_2) = 0.33$ mol%), (b) C_2H_5 radical at $\lambda = 340.8$ nm (laser energy = 8.5 mJ, $p = 1.5$ 0 mbar, $x(C_2H_6) = 1.10$ mol%, $x(F_2) = 0.17$ mol%), (c) difference of the mass spectra for the condition "$C_2H_5 + O$" and "C_2H_5, absence of O atoms spectrum (b)" (conditions of (b), $x(O_2) = 0.09$ mol%), (d) C_2H_5 replaced by C_2D_5 ($p = 1.73$ mbar, $x(C_2D_6) = 0.64$ mol%, $x(F_2) = 0.14$ mol%, $x(O_2) = 0.18$ mol%).

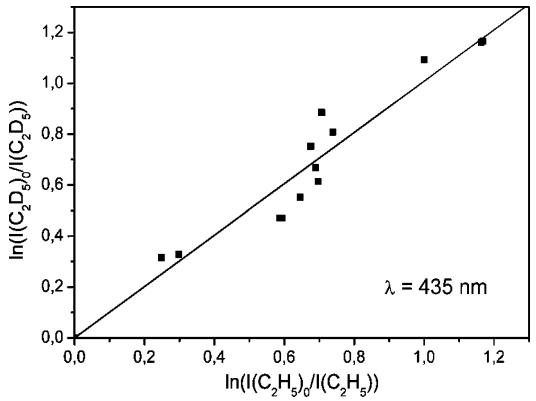

Fig. 8 The reactions $C_2H_5 + O$ and $C_2D_5 + O$: determination of the relative rate coefficients of the reactions $C_2D_5 + O$ and $C_2H_5 + O$ by the consumption of the radicals for increasing amounts of O atoms. Arrangement (C): $\lambda = 435.0$ nm, laser energy = 13 mJ, $p = 1.73$ mbar, $T = 298$ K, $x(C_2H_6) = x(C_2D_6) = 0.69$ mol%, $x(F_2) = 0.15$ mol%; $x(O_2) = 0$–0.22 mol%.

kinetically well-controlled value is chosen as the basis for the further evaluation.

In order to assess the influence of parallel and consecutive reactions on the measured value of k_1/k_{2D}, simulations of the concentration profiles of a number of species have been performed (see Table 3 and Fig. 10). The low concentrations of the indicative species (*e.g.* $CH_3C_2D_5$, C_2H_6) formed in the interfering reactions suggest a marginal influence on the rate determination. Quantitatively this leads to a correction of the apparent ratio (k_1/k_{2D}) by a factor of 1.027 (*i.e.* 2.7% higher). The directly measured rate coefficient k_2 is reported as $(1.04 \pm 0.1) \times 10^{14}$ cm^3 mol^{-1} s^{-1} (ref. 18). Thereby the absolute value of k_1 is deduced from $k_1 = (k_1/k_{2D}) \cdot (k_{2D}/k_2) \cdot k_2$ and, together with the combined error, as $k_1 = (7.6 \pm 1.4) \times 10^{13}$ cm^3 mol^{-1} s^{-1}.

This value is in remarkable good agreement with the latest experimental value of Fockenberg and Preses[10] ($k(300\ K) = (7.34 \pm 0.92) \times 10^{13}$ cm^3 mol^{-1} s^{-1}) and the quantum chemical calculation of Harding *et al.*[14] ($k(300\ K) = 9.26 \times 10^{13}$ cm^3 mol^{-1} s^{-1}). Moreover, the negligible isotope effect of the rate coefficient $k(CD_3 + O)$ is confirmed.

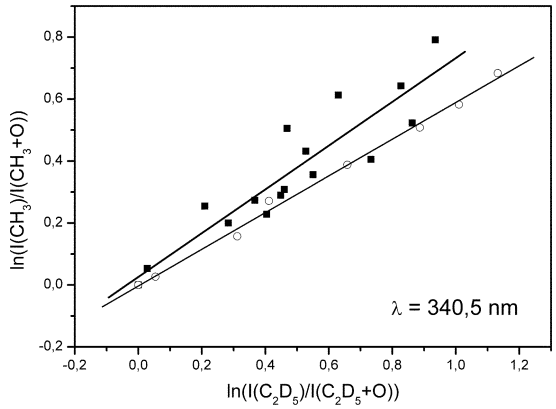

Fig. 9 The reactions $CH_3 + O$ and $C_2D_5 + O$: determination of the relative rate coefficients of the reactions $CH_3 + O$ and $C_2D_5 + O$ by the consumption of the radicals for increasing amounts of O atoms (arrangement (C), $\lambda = 340.5$ nm). "Very low radical concentration" (empty circles): $p = 1.50$ mbar, $T = 298$ K, $[CH_4]_0 = 5.05 \times 10^{-10}$, $[C_2D_6]_0 = 4.04 \times 10^{-10}$, $[F]_0 = 2.55 \times 10^{-11}$ and $[O]_0 = 0$–1×10^{-10} mol cm^{-3}. "Low radical concentration" (filled squares): $p = 1.73$ mbar, $T = 298$ K, $[CH_4]_0 = 3.61 \times 10^{-10}$, $[C_2D_6]_0 = 4.38 \times 10^{-10}$, $[F]_0 = 1.46 \times 10^{-10}$ and $[O]_0 = 0$–1.25×10^{-10} mol cm^{-3}.

Table 3 The reaction $CH_3 + O$ and $C_2D_5 + O$: the mechanism. Data compiled from refs. 15 and 25

Reaction			k/cm^3 mol^{-1} s^{-1}
$CH_4 + F$	→	$CH_3 + HF$	4.72×10^{13}
$CH_3 + CH_3$	→	C_2H_6	2.11×10^{13}
$C_2D_6 + F$	→	$C_2D_5 + DF$	6.00×10^{13}
$C_2D_5 + C_2D_5$	→	C_4H_{10}	1.02×10^{13}
$C_2D_5 + CH_3$	→	$C_2D_5CH_3$	2.85×10^{13}
$C_2H_6 + F$	→	$C_2H_5 + HF$	6.00×10^{13}
$C_2H_5 + C_2H_5$	→	C_4H_{10}	1.02×10^{13}
$C_2H_5 + CH_3$	→	C_3H_8	2.85×10^{13}
$CH_3 + O$	→	$HCHO + H$	4.16×10^{13}
$CH_3 + O$	→	$CO + H_2 + H$	3.44×10^{13}
$CD_3 + O$	→	$DCDO + D$	4.16×10^{13}
$CD_3 + O$	→	$CO + D_2 + D$	3.44×10^{13}
$CD_2H + O$	→	$HCDO + D$	4.15×10^{13}
$CD_2H + O$	→	$CO + D_2 + H$	3.40×10^{13}
$C_2H_5 + O$	→	$HCHO + CH_3$	3.39×10^{13}
$C_2H_5 + O$	→	$CH_3CHO + H$	4.58×10^{13}
$C_2H_5 + O$	→	$C_2H_4 + OH$	2.50×10^{13}
$C_2D_5 + O$	→	$DCDO + CD_3$	3.39×10^{13}
$C_2D_5 + O$	→	$CD_3CDO + D$	4.58×10^{13}
$C_2D_5 + O$	→	$C_2D_4 + OD$	2.50×10^{13}
$C_2H_6 + OH$	→	$C_2H_5 + H_2O$	1.61×10^{11}
$C_2D_6 + OD$	→	$C_2D_5 + D_2O$	1.61×10^{11}
$CH_3 + D$	→	$CH_2D + H$	1.00×10^{14}
$CH_3 + H$	→	CH_4	3.32×10^{12}
$C_2D_5 + D$	→	$CD_3 + CD_3$	3.61×10^{13}
$C_2D_5 + H$	→	$CD_3 + CD_2H$	3.61×10^{13}
$C_2H_5 + H$	→	$CH_3 + CH_3$	3.61×10^{13}

Application

The methane–air flame is the simplest hydrocarbon–air flame and as such has attracted attention for several reasons (natural gas combustion, safety management in mines, flame structure investigations—microprobes, molecular beam mass spectrometry, laser based diagnostics—and modelling studies of this basic flame being used as a model for more complex fuel flames). An interesting account of the development of the knowledge of methane-flame structure and the inherent chemical processes is given in ref. 30 (see also ref. 31, and the discussion therein). In the context of the present study a few details are mentioned. It is generally accepted that the primary attack of CH_4 is by atoms and radicals leading to CH_3 radicals, which in lean and stoichiometric flames, react with O atoms. From the early formation of CO in a flame two possible pathways have been suggested: HCHO + M → CO +

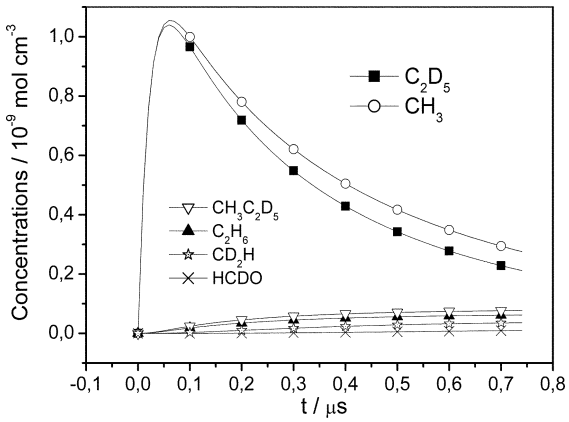

Fig. 10 The reactions $CH_3 + O$ and $C_2D_5 + O$: modeling of the concentration/time profiles of the species assuming the reactions of Table 3 and the experimental conditions of Fig. 9 ($[CH_4]_0 = 5.05 \times 10^{-10}$, $[C_2D_6]_0 = 4.04 \times 10^{-10}$, $[F]_0 = 2.55 \times 10^{-11}$and $[O]_0 = 3.06 \times 10^{-11}$ mol cm^{-3}).

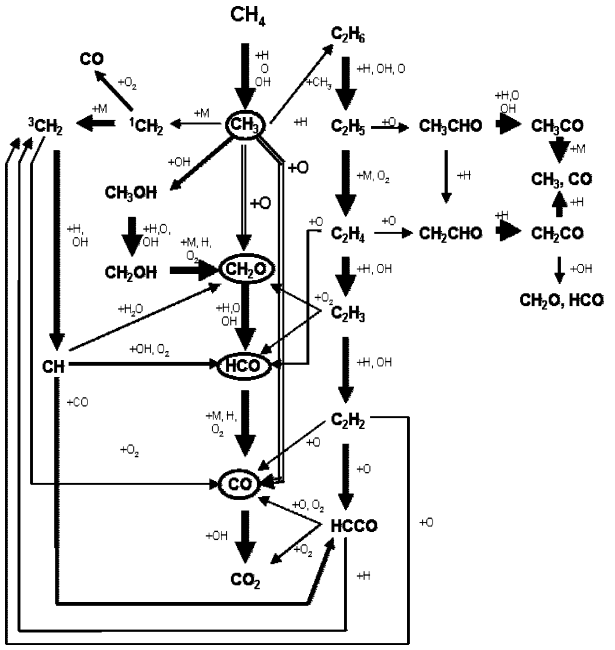

Fig. 11 Atmospheric stoichiometric laminar CH_4–air flame: integral chemical flow analysis. The thickness of the arrows indicates the significance of a reaction path: 100–75% (very thick); 75–50% (thick); 50–25% (thin) and 25–5% (very thin).

H_2 and a route *via* HCO. Whereas early measurements on $CH_3 + O$ indicate the sole formation of HCHO, IR chemiluminescence studies[6] of CO($v = 1, 2, ...$) gave a 40% route to CO + H_2 + H (being adopted in the GRI mechanism[16]) and suggest a mechanism which is broadly validated for flame speeds, structures and ignition delay times of C1–C4 hydrocarbons.[32] This mechanism has been applied to perform an integral reaction flow analysis of a stoichiometric CH_4–air flame at atmospheric pressure (see Fig. 11, ref. 33) in which the presented data on the rate coefficient of the reaction $CH_3 + O$ and the channel branching have been included. The simulation shows that in the first step 95% of the fuel loses an H atom and forms CH_3 of which 50% is directly oxidized by O atoms. Fig. 11 shows the results of flame-structure simulations with respect to the HCHO concentrations. Five simulations were performed with fractions of the HCHO forming channel of 100%, 80%, 60%, 40% and 20%. In all cases the total rate coefficient $k(CH_3 + O \rightarrow$ products) is taken from this study. The predicted HCHO concentration profiles are shown in Fig. 12. The high sensitivity of the two reaction routes ($O + CH_3 \rightarrow$ HCHO + H/CO + H_2 + H) for predicting concentrations of the key

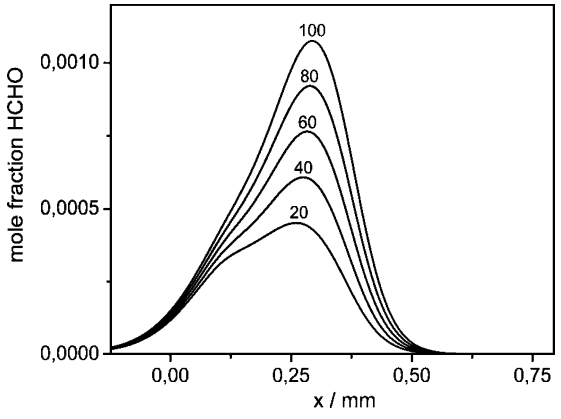

Fig. 12 Simulations of HCHO concentration profiles in an atmospheric stoichiometric CH_4–air flame as a function of height above the burner for different branching ratios $k_1(a1)/(k_1(a1) + k_2(a2)) = 100\%$, 80%, 60%, 40%, 20%; $k_1(a1) + k_2(a2) = 7.6 \times 10^{13}$ cm^3 mol^{-1} s^{-1}.

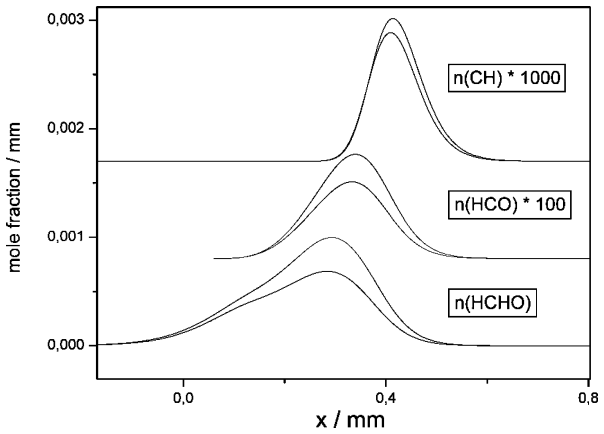

Fig. 13 Simulations of HCHO, HCO (offset 0.008, scaling factor 100) and CH (offset 0.0017, scaling factor 1000) mole fraction profiles in an atmospheric stoichiometric CH_4–air flame as a function of height above the burner for branching ratios $k_1(a1)/(k_1(a1) + k_2(a2)) = 10\%$ (case I) and 50% (case II); $(k_1(a1) + k_2(a2) = 7.6 \times 10^{13}$ cm^3 mol^{-1} s^{-1}. Profiles for case I are always higher than for case II.

intermediate HCHO under flame conditions is obvious since there is a factor of almost three between the maximum HCHO concentration for the 100% and the 20% case. A high sensitivity to the CO channel fraction is also seen in the concentration profiles of the important intermediate species HCO and CH. Here calculations were performed with CO channel fractions of 10%, case I, and 50%, case II, being, respectively, the lower and upper limit given in ref. 10 and in this study. As HCO is mainly formed by HCHO decomposition, its maximum HCHO concentration is lowered to the same extent as expected when calculation are performed for the cases I and II. But also minor species, not directly formed from CH_3 or HCHO, are affected. The CH concentration for example is reduced by 20% when applying case I instead of II. These results are illustrated in Fig. 13. The CO concentration profiles show only minor differences with a slightly higher and earlier CO peak in case II. But the flow analysis reveals that in this case (II) 50% of CO is formed from CH_3 while only 12% is predicted in case I.

The flame-structure analysis shows that the reaction flow of the important intermediate species CH_3, HCO, and HCHO is strongly influenced by the CO channel fraction of the title reaction. But also minor species such as CH are coupled to the CO channel fraction. All calculations point to the necessity of the inclusion of a kinetically verified mechanism and rate of the reaction $CH_3 + O$.

Details of the mechanism, the modeling of measured species concentrations in flames, the calculation of burning velocities, and ignition delay times are given in refs. 32 and 33.

Acknowledgements

This work was financially supported by the European Community IHP programme "Marie Curie Fellowships" through contract number HPMT-CT-2000–00080 (FP-5). Funding by the Deutsche Forschungsgemeinschaft (SFB 357 "Molekulare Mechanismen unimolekularer Prozesse") is also gratefully acknowledged.

References

1 J. Warnatz, U. Maas and R. W. Dibble, *Combustion*, Springer, Berlin, 1996.
2 K. Hoyermann and R. Sievert, *Proc. Combust. Inst.*, 1978, **17**, 517.
3 I. R. Slagle, D. Sarzynski and D. Gutman, *J. Phys. Chem.*, 1987, **91**, 4375.
4 R. Zellner, D. Artmann, J. Karthäuser, P. Rhäsa and G. Weibring, *J. Chem. Soc., Faraday Trans. 2*, 1988, **84**, 549.
5 A. M. Dean and P. R. Westmoreland, *Int. J. Chem. Kinet.*, 1987, **19**, 207.

6 P. W. Seakins and S. R. Leone, *J. Phys. Chem.*, 1992, **96**, 4478.
7 C. Fockenberg, G. E. Hall, J. M. Preses, T. J. Sears and J. T. Muckerman, *J. Phys. Chem. A*, 1999, **103**, 5722.
8 M. Preses, C. Fockenberg and G. W. Flynn, *J. Phys. Chem. A*, 2000, **104**, 6758.
9 T. P. Marcy, R. R. Diaz, D. Heard, S. R. Leone, L. B. Harding and S. J. Klippenstein, *J. Phys. Chem. A*, 2001, **105**, 8361.
10 C. Fockenberg and J. M. Preses, *J. Phys. Chem. A*, 2002, **106**, 2924.
11 W. Hack, K. Hoyermann, M. Olzmann and T. Zeuch, *Proc. Combust. Inst.*, 2002, **29**, 1255.
12 H. Oser, D. Walter, N. D. Strothard, O. Grotheer and H. H. Grotheer, *Chem. Phys. Lett.*, 1991, **181**, 521.
13 C. N. Washida and S. Inomata, *16th Symposium on Gas Kinetics*, the Gas Kinetics Group of the Faraday Division of the Royal Society of Chemistry, Cambridge, UK, 2000, p. C6.
14 L. B. Harding, S. J. Klippenstein and Y. Georgieskii, *Proc. Combust. Inst.*, 2004, **30**, 985–993.
15 D. L. Baulch, C. J. Cobos, R. A. Cox, P. Frank, G. Hayman, T. Just, J. A. Kerr, T. Murrells, M. J. Pilling, J. Troe, R. W. Walker and J. Warnatz, *J. Phys. Chem. Ref. Data*, 1994, **23**, 847.
16 G. P. Smith, D. M. Golden, M. Frenklach, N. W. Moriarty, B. Eiteneer, M. Goldenberg, C. T. Bowman, R. K. Hanson, S. Song, W. C. Gardiner, Jr., V. V. Lissianski and Z. Quin, http://www.me.berkeley.edu/gri_mech/.
17 W. Hack, K. Hoyermann, C. Kersten, M. Olzmann and B. Viskolcz, *Phys. Chem. Chem. Phys.*, 2001, **3**, 2365.
18 W. Hack, K. Hoyermann, M. Olzmann and T. Zeuch, *Proc. Combust. Inst.*, 2002, **29**, 1247.
19 K. Hoyermann, M. Olzmann, J. Seeba and B. Viskolcz, *J. Phys. Chem. A*, 1999, **103**, 5692.
20 K. Hoyermann and F. Nacke, *Proc. Combust. Inst.*, 1996, **26**, 505.
21 T. Muller, P. H. Vaccaro, F. Perez-Bernal and F. Iachello, *J. Chem. Phys.*, 1999, **111**, 5038.
22 T. Shimanouchi, *Tables of Molecular Vibrational Frequencies Consolidated Volume I*, National Bureau of Standards, 1972, 1–160.
23 I. R. Slagle, D. Sarzyński, D. Gutman, J. A. Miller and C. F. Melius, *J. Chem. Soc., Faraday Trans.*, 1988, **84**, 491.
24 M. K. Gilles, A. A. Turnipseed, R. K. Talukkdar, Y. Rudich, P. W. Villalta, L. G. Huey, J. B. Burkholder and A. R. Ravishankara, *J. Phys. Chem.*, 1996, **100**, 14005.
25 NIST Standard Reference Database 17, *NIST Chemical Kinetics Database: Version 2Q98e*, 1998.
26 F. Maguin, A. Mellouki, G. Laverdet, G. Poulet and G. Le Bras, *Int. J. Chem. Kinet.*, 1991, **23**, 237.
27 J. W. Lindner, R. A. Loomis, J. J. Klaasen and S. R. Leone, *J. Chem. Phys.*, 1998, **108**, 1944.
28 J. P. Reid, T. P. Marcy, S. Kuehn and S. R. Leone, *J. Chem. Phys.*, 2000, **113**, 4572.
29 J. W. Hudgens, in *Advances in Multi-photon Processes and Spectroscopy*, ed. S. H. Lin, World Scientific, Singapore, **vol. 4**, 1988, p. 171.
30 R. M. Fristrom, *Flame Structure and Processes*, Oxford University Press, New York, 1995, p. 323.
31 J. Peeters and G. Mahnen, *Proc. Combust. Inst.*, 1973, **14**, 133–146.
32 K. Hoyermann, F. Mauß and T. Zeuch, *Phys. Chem. Chem. Phys.*, 2004, **6**, 3824.
33 T. Zeuch, Reaktionskinetik von Verbrennungsprozessen in der Gasphase: Spektroskopische Untersuchungen der Geschwindigkeit, Reaktionsprodukte und Mechanismen von Elementarreaktionen und die Modellierung der Oxidation von Kohlenwasserstoffen mit detaillierten Reaktionsmechanismen, , PhD thesis, University of Göttingen, Germany, 2003.

